THE AMERICAN MINERALOGIST, VOL. 43, MARCH-APRIL, 1958

TWINNING IN DIAMOND-TYPE STRUCTURES: A PROPOSED BOUNDARY-STRUCTURE MODEL*

J. A. KOHN, *U. S. Army Signal Engineering Laboratories, Fort Monmouth, N. J.*

ABSTRACT

Lateral twin boundaries (twin plane and boundary plane not coincident), second-order twin joins (boundaries between individuals related by two non-parallel stages of twinning), and probable third-order twin joins have been observed in silicon. Their directions are restricted to rows of sites in a coincidence site superlattice (net of positions common to both individuals of the twin). Using (110)-projected coincidence nets, seven *permissible* ($hh\bar{l}l$) boundaries can be derived (four first-order and three second-order); these have high coincidence site density and their trans-boundary structure is "restorable" to a considerable degree if the discontinuity zig-zags, or oscillates between two (or three) simple crystallographic directions in each case. By using a zig-zag discontinuity as a "restoration" mechanism, trans-boundary deviations from undistorted bonding are minimized, and a preferred growth along these directions is to be expected. The seven proposed boundaries are

First-Order	*Second-Order*
{115}-{111}	{221}-{221}
{112}-{112}	{115}-{111}
{001}-{221}	{114}-{114}
{110}-{114}	

Constructions are presented showing the proposed, ideal, detailed structure for the seven boundaries. Six of these seven have been observed experimentally in the same silicon specimen. *No other* first- or second-order discontinuities were found.

Grain boundary energy relationships are discussed; reference is made to implications on semiconductor properties.

INTRODUCTION

Interest has been focussed recently on the crystallography of diamond-type materials, especially silicon and germanium, owing to their use in semiconductor devices. The proper functioning of such devices depends, in part, upon the crystalline perfection of the material involved, and to this end, the defect structure of diamond-type crystals has come under close scrutiny. Twinning, of course, is a defect, and as such it is a possible deterrent to structure-sensitive electrical properties (1), e.g., lifetime of minority carriers and carrier mobility.

As discussed by Slawson (2), diamond crystals are predisposed to twinning. As expected, silicon and germanium, both of which are isomorphous with diamond, also show high degrees of twinning. Further, diamond and silicon have been shown to exhibit more complex, high-order twinning (2) (3) (4), a feature which undoubtedly is also displayed by ger-

* Presented at Fourth International Congress, International Union of Crystallography, Montreal, Canada, July, 10–19 1957.

manium. Simple first-order twinning, where twin plane (invariably (111) for these materials) and composition plane are coincident, gives rise to only a slight structure discontinuity. Structure-sensitive electrical properties are expected to be essentially unaffected. Most workers agree that even lifetime of minority carriers, the most structure-sensitive electrical property, is not altered in such a case (5). It might be expected that multiple parallel twinning of this type would have an effect on lifetime; experimental data, however, are not available. It has been shown by the use of an infrared image tube that multiple parallel twinning gives rise to an observable birefringence, probably deriving from the cumulative effect of the anisotropic (hexagonal) lamellae introduced by the twinning operations (6).

A structure discontinuity of somewhat higher degree would be expected in the case of first-order twinning if the twin plane and composition plane are not coincident. Such *lateral* (also referred to as "semicoherent," "noncoherent," and "incoherent") twin boundaries have been discussed by Ellis and Treuting (7) for cubic crystals and reported in several materials. They have been observed in silicon during the present study and are described herein. Lateral twin boundaries, since they entail a greater deviation from undistorted bonding than those in which twin plane and composition plane are coincident, are expected to have a somewhat greater effect upon structure-sensitive electrical properties; no direct measurements, however, are available.

Other structure discontinuities are generated by high-order twinning. A diamond-type crystal, I, twins and the resultant individual, II, twins again (non-parallel) to generate a third crystal, III. Should I and III then become contiguous, the boundary along which contact is made is termed a second-order twin join (4). Similarly, should the individuals making contact be related by three stages of non-parallel twinning, a third-order join is developed. As the order of the particular twin join increases, deviation from undistorted bonding becomes greater, and the effect on structure-sensitive electrical properties is expected to increase. Finally, after four stages of twinning, there are no longer any lattice sites common to both individuals (see discussion below), and the discontinuity probably approaches that of a common grain boundary having high energy. High-energy grain boundaries are of practical importance for certain semiconductor device applications (8).

Grain boundary energy, as described by Read (9), is comprised of two types: the energy of atomic disorder and the energy of elastic deformation. Read and Shockley (10) have correlated grain boundary energy with the angle of misfit between the two crystals. Expressed in terms of bonding, it would seem that as the specific deviations from undistorted

bonding increase, the energy of the particular grain boundary increases. In other words, the greater the degree to which the trans-boundary structure can be "restored" to the undistorted state, the lower the associated energy.

A general grain boundary has five degrees of freedom. In the case of a discontinuity derived by twinning, three of these degrees of freedom are established; the two remaining are associated with the orientation of the surface along which the two individuals make contact. To determine the possible orientations of such a surface, consider the "interpenetrated" lattices of two individuals twinned with respect to each other. Certain atomic sites are common to both structures, and these sites form a net, which Ellis and Treuting have referred to as a coincidence site superlattice (7). First-order twinning has associated with it a specific coincidence superlattice, which differs from those accompanying second- and third-order twinning. With fourth- and presumably higher-order twinning of a diamond-type structure, there are no lattice points common to both individuals and therefore no coincidence site superlattice exists. A given twin boundary will tend to contain lattice sites common to both individuals, that is to orient itself along rows of sites in the coincidence net. In so doing, it would tend to minimize deviations from an undistorted structural array and thus lower its associated energy. Lattice site directions in the coincidence site superlattice, then, represent cusps or minima in the curve relating grain boundary energy and boundary direction.

The coincidence net, of course, is three-dimensional. The problem can be simplified with a two-dimensional approach. First-order twinning in the diamond structure can be interpreted geometrically as a rotation about [110] of 70°32′. Further, second- and third-order twinnings can be considered as rotations about [110] of 38°57′ and 31°35′, respectively. Superposed (110) projections, rotated by the proper amount, give two-dimensional coincidence site superlattices which are constant-projecting along the third direction, [110]. Restriction to such a two-dimensional net, in effect, eliminates one of the two degrees of freedom associated with the boundary surface. It is sufficient, nevertheless, to describe the model Actually, in practice, one of these two degrees of freedom is somewhat controlled during growth of the crystals: the two most widely used methods for growing single crystals of silicon today, the Czochralski technique (pulling from a melt) (11) and the floating zone method (moving a molten zone vertically through an ingot) (12), both impart a strong unidirectional temperature gradient to the crystal, and it has been shown that twin boundaries in silicon tend to follow the temperature gradient (13).

Examination of superposed (110) projections (first- and second-order

twinning) reveals that only in case of the usual first-order twinning, with twin plane and composition plane coincident, can a "restorable" (cf. section on *First-Order Twinning*) *straight line* boundary be drawn.* As is well known, the restoration in this case is nearly complete, involving deviations commencing with the third coordination sphere. In the case of lateral twin boundaries and second-order twin joins, "restorable" boundaries can be attained if a type of oscillating, or *zig-zag* discontinuity

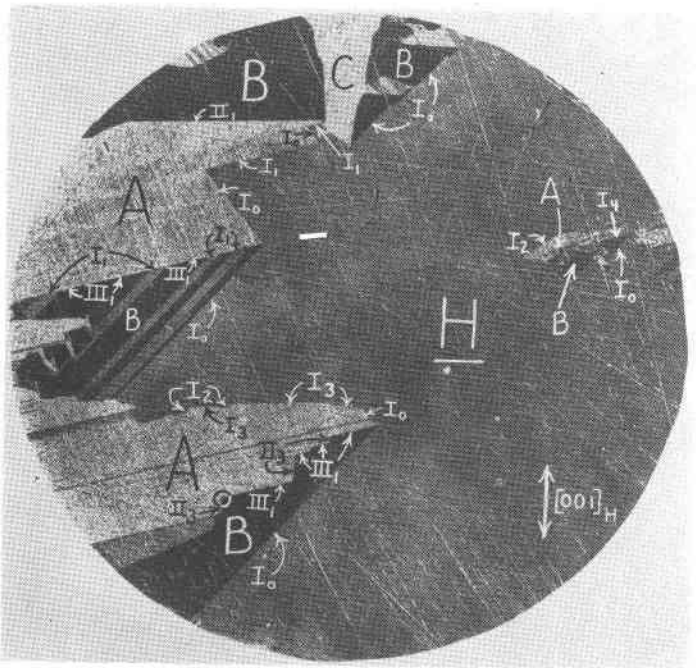

FIG. 1. Silicon crystal section, viewed approximately along [110], showing host, twins, and observed boundaries; see text for explanation of symbols. 9×.

is employed. The resultant directions of such zig-zag discontinuities follow rows of lattice sites in the respective coincidence net.

EXPERIMENTAL RESULTS

Figure 1 shows an etched section of a silicon crystal. The crystal was grown by pulling from a melt along [100]; the section is viewed approximately along [110]. The dark gray area (bulk of the section) is the host crystal, H; the light gray and black areas are mainly first-order twins

* Refer to discussion of the {112}-{112} lateral twin boundary (*First-Order Twinning* section) for qualification of this statement.

with respect to the host. Specifically, the light gray regions designated A are twinned on $(\bar{1}11)$ of the host; the black areas, labelled B, are twinned on $(1\bar{1}1)$; the light gray area designated C is twinned on (111). The host, A, and B have a common (110) approximately in the plane of the figure and are amenable to the two-dimensional treatment using superposed (110) projections. The discussion will therefore be limited to these orientations.

TABLE 1. PROPOSED AND OBSERVED $(h\bar{h}l)$ BOUNDARIES

	Proposed from Model	Experimentally Observed	Figure 1 Designation
First Order	{115}-{111}	{115}-{111}	I_1
	{112}-{112}	{112}-{112}	I_2
	{001}-{221}	{001}-{221}	I_3
	{110}-{114}	{110}-{114}	I_4
Second Order	{221}-{221}	{221}-{221}	II_1
	{115}-{111}	not found	—
	{114}-{114}	{114}-{114}	II_3

The twinning relationships among the crystallographic areas of Fig. 1, as well as the directions of the various boundaries, were established by x-ray diffraction, using the back-reflection Laue method. For consistency with the two-dimensional treatment used herein, the relatively few boundaries oblique to the plane of the figure, i.e., other than $(h\bar{h}l)$, were not considered. In addition to the normal first-order twinning case, wherein twin plane and composition plane are coincident, four lateral twin boundaries of the type $(h\bar{h}l)$, i.e., containing [110], were found. Indexed with respect to the axes of both host and twin, they are {115}-{111}, {112}-{112}, {001}-{221}, and {110}-{114}. These lateral twin boundaries are designated I_1, I_2, I_3, and I_4, respectively, in Fig. 1; the normal case is designated I_0. Examination of boundaries between individuals related by two orders of twinning showed two $(h\bar{h}l)$ second-order twin joins, {221}-{221} and {114}-{114}. These are designated II_1 and II_3, respectively, in Fig. 1. The observed boundaries for first- and second-order twinning are listed in Table 1 and compared with those derived by purely theoretical considerations using the proposed model (see subsequent sections for derivation and discussion); the appropriate designations for Fig. 1 are also listed.

No other $(h\bar{h}l)$ first-order lateral twin boundaries or second-order twin joins were experimentally observed in the present study. One additional set of boundaries, however, was found (cf. III_1, Fig. 1). Although these

seemed at first to be second-order twin joins having a direction contrary to the proposed model, examination under high magnification showed that they were probably higher-order twin joins. These boundaries are discussed in detail in the section on *Third-Order Twinning*.

First-Order Twinning

Figure 2 shows the coincidence site superlattice for first-order twinning derived by rotating superposed (110) projections by 70°32′ about [110]. Only sites common to both individuals are shown; intervening

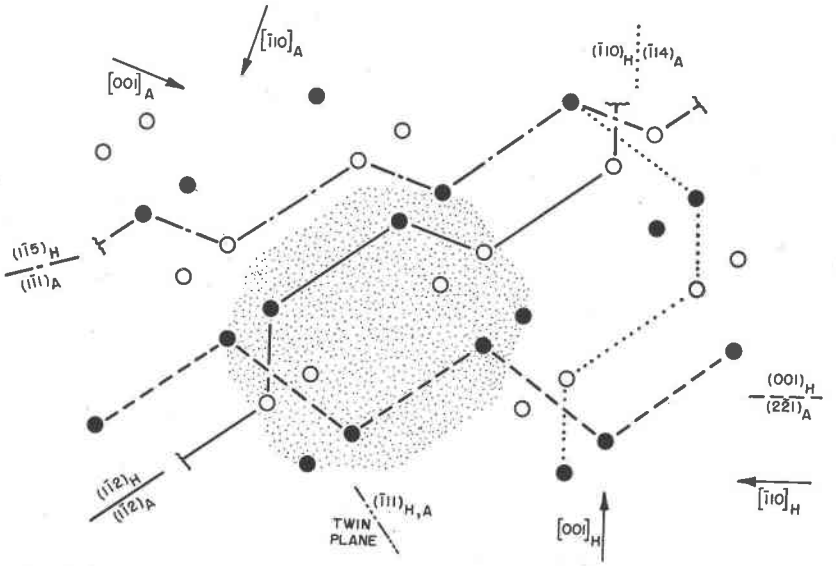

Fig. 2. (110)-projected coincidence site superlattice for first-order twinning, showing traces of proposed ($h\bar{h}l$) lateral twin boundaries.

atomic positions of the "interpenetrated" twin pair have been omitted. Crystallographic directions of the host individual, H, and individual A, generated by twinning on $(\bar{1}11)$, are noted for correlation with subsequent diagrams. Solid symbols represent sites in the plane of the drawing; open symbols refer to sites $\sqrt{2}\ a_0/4$ above (or below) the plane of the figure.

As stated previously, a boundary will tend to orient itself along rows of sites in the coincidence net, in order to minimize its associated energy. It would seem, also, that the resultant discontinuity should be such that its trans-boundary structure can be rebuilt, or *restored* to a state approaching normalcy. The proposed boundary-structure model is based on the

requirements of (*a*) high coincidence site density and (*b*) a considerable degree of trans-boundary structural restoration. These conditions can be satisfied simultaneously if the discontinuity zig-zags between restorable, inter-site segments in the coincidence net. What restorable segments are available to such a zig-zag discontinuity?

The stippled area of Fig. 2 is reproduced in Fig. 3*a* to show the complete, "interpenetrated" structures. From coincidence site 1, the boundary can proceed along segments to coincidence positions 2, 3, 4, 5, 6, or 7. Excepting symmetrically equivalent segments, other directions are

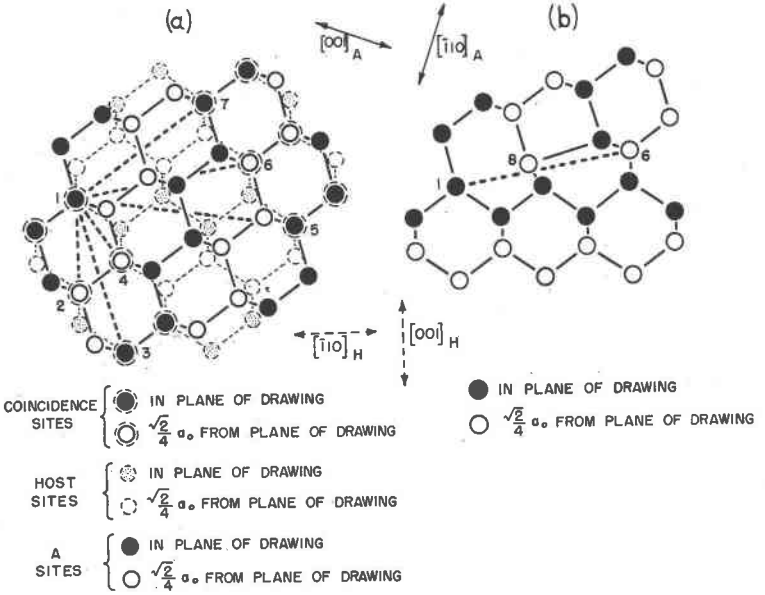

FIG. 3. (*a*) Detail of stippled area in Fig. 2, showing complete "interpenetrated" structures and possible boundary segments. (*b*) A reconstructed 1–6 vector, exemplifying a "non-restorable" boundary segment.

eliminated owing to requirement (*a*) above, i.e., higher coincidence site density. Do the six available segments permit structural restoration when used in actual boundaries? The discontinuity illustrated in Fig. 5 (see ahead) uses segments 1–2 (short) and 1–7 (long). A considerable degree of structural restoration has been achieved; these are "restorable" segments. The boundary in Fig. 6 uses a segment symmetrically equivalent to 1–3 as its NW-SE component; this is also a restorable segment. On the other hand, 1–5 and 1–6 are "non-restorable" segments. This is illustrated in Fig. 3b, using 1–6. Substantial deviations from normal

bonding result (note position 8); the trans-boundary structure cannot be suitably restored. Use of the 1–4 segment, or longer segments having the same direction, results in a boundary which degenerates either to the usual $\{111\}$-$\{111\}$ twin boundary or to a discontinuity employing the restorable segments mentioned above.

Using simple combinations of the three established restorable segments, four $(h\bar{h}l)$ zig-zag discontinuities were found representing permissible lateral twin boundaries.* Indexed with respect to the axes of both individuals, the resultant directions of these boundaries lie along $(1\bar{1}5)_H$-

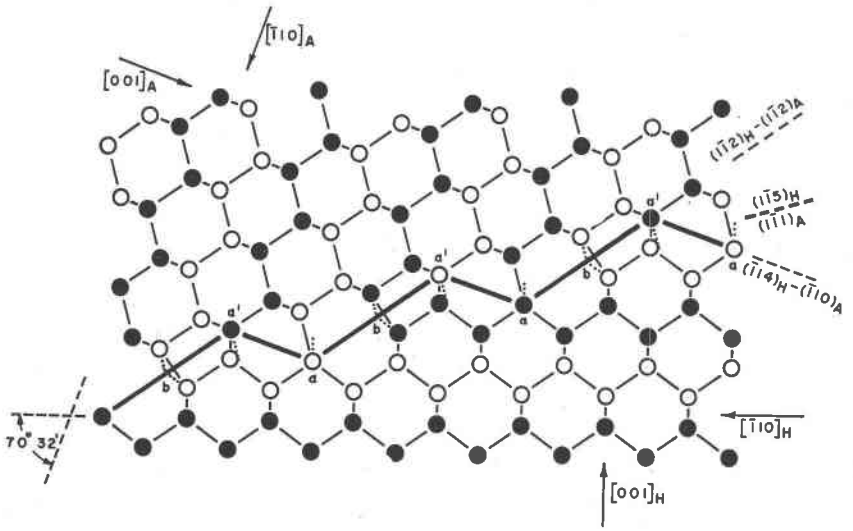

FIG. 4. {115}-{111} lateral twin boundary; see text for symbol explanation.

$(1\bar{1}1)_A$, $(1\bar{1}2)_H$-$(1\bar{1}2)_A$, $(001)_H$-$(2\bar{2}1)_A$, and $(\bar{1}10)_H$-$(\bar{1}14)_A$. Their relationship to the coincidence net is shown in Fig. 2. With the exception of more complex boundaries using combinations of these four, no other permissible $(h\bar{h}l)$ lateral twin boundaries could be found which satisfied the requirements of the model.

Figures 4, 5, 6, and 7 show the proposed, ideal, detailed structure of the four restored lateral twin boundaries. The zig-zag discontinuity having a resultant direction along $(1\bar{1}5)$ of the host and $(1\bar{1}1)$ of individual A is shown in Fig. 4. The host structure, below the discontinuity, is related to that of A, above the boundary, by a rotation of 70°32′ about a

* A three dimensional analysis would include a permissible {110}-{110} boundary (in the plane of Fig. 2); such a boundary has been observed in copper (14) and indium antimonide (15). Also, Churchman, Geach, and Winton (16) mention {123}-{321} and {201}-{021} "semi-coherent" boundaries for first-order twinning in the diamond structure.

normal to the figure, [110]. The proposed discontinuity oscillates between segments having directions along $(1\bar{1}2)_H$-$(1\bar{1}2)_A$ and $(\bar{1}14)_H$-$(\bar{1}10)_A$ (segment types 1–7 and 1–2, respectively, of Fig. 3*a*). As shown in the construction, the trans-boundary structure is restorable to a considerable degree. Undistorted atomic configuration leads to a six-sided array, as seen projected along [110]. Along unit length (two adjacent segments), the proposed discontinuity offers, instead, an altered six-sided figure followed by a seven- and a five-sided array. Of greater interest in examining deviations from an undistorted atomic configuration is the direction and /or length of specific bonds along the discontinuity. At atomic positions where such changes have taken place, the former bond directions are indicated by dotted lines in the figure. At points designated *a* and *a'*, the bond has been rotated respectively into and out of the plane of the figure by 57°1′. At *b* two bonds have been combined to one, the resultant being approximately 6% shorter than normal; each original bond has been rotated 19°28′ in the plane of the figure. Neglecting the shortened bond, the atoms on either side of position *b* still have four nearest neighbors. Atoms at *a* and *a'*, however, have changed in this respect. Specifically, the *a* positions now require only three nearest neighbors, while the *a'* sites require five nearest neighbors. The *a* and *a'* positions in Fig. 4 are third nearest neighbors; the paired separation is $0.829a_0$ or 1.9 times the usual bond length ($0.433a_0$). The proximity of these abnormally coordinated sites allows for an adjustment of the structure to alleviate the condition. In other words, there should be a tendency for one of the bonds directed at *a'* to be redirected toward *a*. Additional, more subtle adjustments of the structures on either side of the discontinuity should be expected in order to accommodate the proposed boundary changes. A considerable degree of restoration, nevertheless, has been achieved, which effectively lowers the energy associated with the discontinuity. This boundary energy is higher than would have been the case if twin plane and composition plane were coincident, but not as high as that associated with a common grain boundary, where restoration is presumably at a minimum. See Table 1 and Fig. 1 for comparison with experimental results.

The second lateral twin boundary, that having a resultant direction along $(1\bar{1}2)$ of the host and $(1\bar{1}2)$ of individual A, is shown in Fig. 5. The relative orientations of host and A are precisely the same here as in the previous construction. The discontinuity oscillates, as shown, among segments having directions along $(\bar{1}14)_H$-$(\bar{1}10)_A$, $(1\bar{1}2)_H$-$(1\bar{1}2)_A$, and $(\bar{1}10)_H$-$(\bar{1}14)_A$ (segment types 1–2, 1–7, and 1–2, respectively, of Fig. 3*a*). Along unit length of the discontinuity, i.e., two adjacent segments, the projected atomic configuration shows an altered six-, a seven-, and a

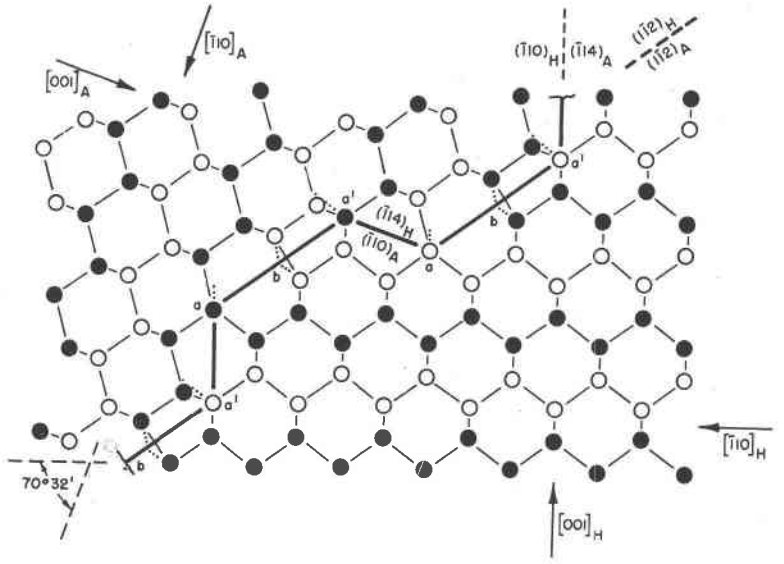

FIG. 5. {112}-{112} lateral twin boundary.

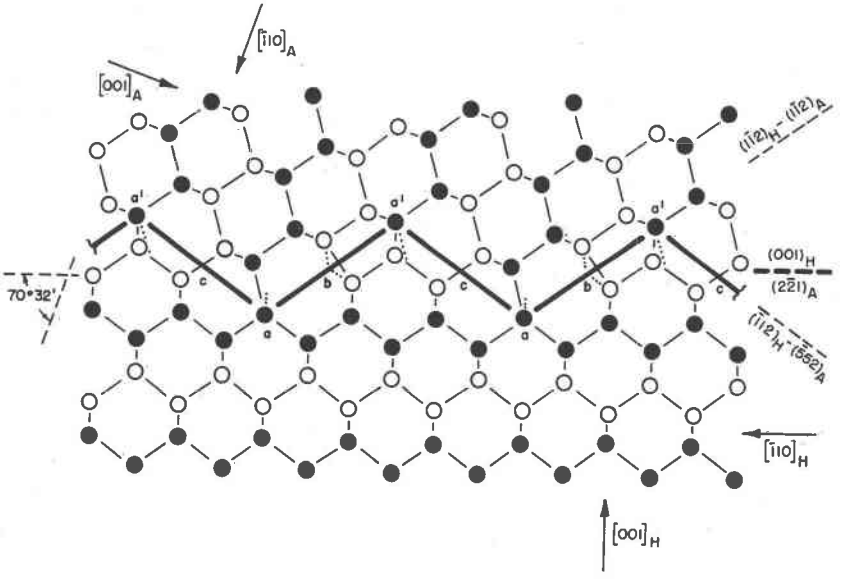

FIG. 6. {001}-{221} lateral twin boundary.

five-sided array, in this respect being the same as the $\{115\}$-$\{111\}$ discontinuity. In fact, the specific bonding changes indicated at positions a, a', and b are the same as at the similarly designated positions in Fig. 4.* Comparison between the $\{115\}$-$\{111\}$ and $\{112\}$-$\{112\}$ boundaries reveals that they differ only with respect to the direction reversals shown by the latter. See Table 1 and Fig. 1 for comparison with experimental results; $\{112\}$-$\{112\}$ boundaries have also been observed in silicon by Salkovitz and von Batchelder (17).

Actually, a straight line discontinuity can be constructed as an alternative for the $\{112\}$-$\{112\}$ lateral twin boundary. In this case, however, the sites requiring three and five nearest neighbors are already connected by a bond in the plane of the discontinuity. The actual equilibrium position for the boundary is most probably between the two extremes, i.e., between a straight line discontinuity and that presented in Fig. 5.

The lateral twin boundary having a resultant direction along (001) of the host and $(2\bar{2}1)$ of individual A is shown in Fig. 6. The relative orientations of the two individuals are again the same as in the two cases just discussed. The discontinuity oscillates between segments having directions along $(1\bar{1}2)_H$-$(1\bar{1}2)_A$ and $(\bar{1}12)_H$-$(\bar{5}52)_A$ (segment types 1–7 and 1–3, respectively, of Fig. 3*a*). Two adjacent boundary segments show projected atomic configurations having six, six (both altered), seven, and five sides. Again, specific deviations in bonding noted at positions a, a', and b are the same as in the foregoing two constructions. At c the bond is altered only for third and higher coordinations, i.e., the normal first-order twinning relationship. In the present construction, positions a and a', which require three and five nearest neighbors respectively, are separated by $1.479a_0$ or 3.4 times the usual bond length. This distance is considerably greater than the separation found in the case of the first two lateral twin boundaries ($0.829a_0$). Accordingly, the structural adjustments necessary to accommodate the specified abnormalities are not as easily accomplished. See Table 1 and Fig. 1 for comparison with experimental results.

The fourth lateral twin boundary for first-order twinning is shown in Fig. 7; it has a resultant direction along $(\bar{1}10)$ of the host and $(\bar{1}14)$ of individual A. The boundary oscillates among segments having directions along $(1\bar{1}2)_H$-$(1\bar{1}2)_A$, $(\bar{1}10)_H$-$(\bar{1}14)_A$, and $(\bar{1}12)_H$-$(\bar{5}52)_A$ (segment types 1–7, 1–2, and 1–3, respectively, of Fig. 3*a*). The projected atomic configurations along three successive boundary segments show four altered six-sided arrays followed by two having seven and five sides. The specific

* Ellis and Treuting (7) noted that in the case of a $\{112\}$-$\{112\}$ lateral twin boundary in the diamond structure, atoms on the coincidence plane have alternately three and five nearest neighbors.

bonding deviations noted at a, a', b, and c are as previously indicated. The abnormally coordinated sites a and a', although paired in their distribution along the discontinuity, are separated by 3.4 times the usual bond length. There are less such sites along unit length of the (110)-projected boundary than in the three constructions described above. See Table 1 and Fig. 1 for comparison with experimental results.

From a theoretical point of view, the four discontinuities described

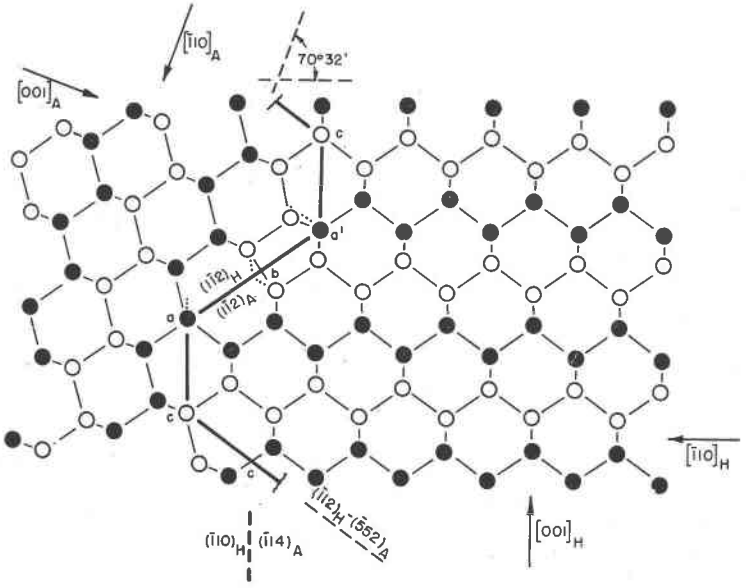

FIG. 7. {110}-{114} lateral twin boundary.

above are the only simple, $(h\bar{h}l)$ lateral twin boundaries susceptible to a considerable degree of structural restoration and having high coincidence site density. One might propose more complicated boundaries based upon combinations of these to varying degrees, but this seems impractical. It appears significant that, among the clearly delineated $(h\bar{h}l)$ lateral twin boundaries found in the specimen (Fig. 1), the $\{115\}$-$\{111\}$, $\{112\}$-$\{112\}$, $\{001\}$-$\{221\}$, and $\{110\}$-$\{114\}$ discontinuities, *and only these*, were observed. Such boundaries, then, have a strong tendency to orient themselves along rows of lattice sites in the coincidence site superlattice for first-order twinning. The zig-zag discontinuity is proposed as a mechanism of restoration, whereby the necessary trans-boundary deviations from an undistorted atomic configuration are minimized and the energy associated with the discontinuity is effectively reduced.

Second-Order Twinning

The coincidence site superlattice for second-order twinning is shown in Fig. 8. It was derived by rotating superposed (110) projections by 38°57′ around [110]. Crystallographic directions are indicated for individual A, generated by twinning on $(\bar{1}11)$ of the host, and for individual B, derived by twinning on $(1\bar{1}1)$ of the host. Comparison with Fig. 2 shows that the coincidence net for second-order twinning has a consider-

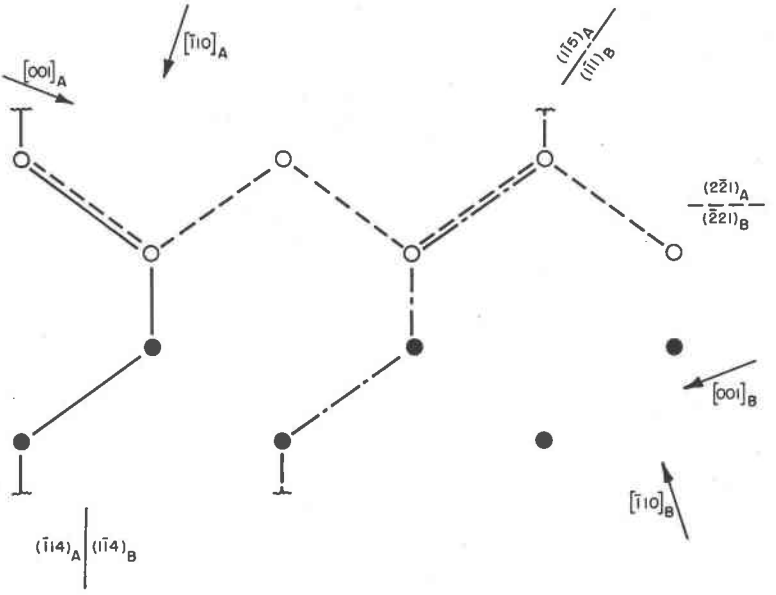

Fig. 8. (110)-projected coincidence site superlattice for second-order twinning, showing traces of proposed $(h\bar{h}l)$ second-order twin joins.

ably lower site density. Using the same requirements as were applied for first-order twinning, it is found that there are but two restorable segments: $(\bar{1}14)_A$-$(1\bar{1}4)_B$ and $(1\bar{1}2)_A$-$(2\bar{2}1)_B$ (or symmetrically equivalent $(\bar{2}21)_A$-$(\bar{1}12)_B$). Simple combinations of these yield three $(h\bar{h}l)$, restorable, zig-zag discontinuities representing permissible second-order twin joins.* Indexed with respect to the axes of both individuals, these have resultant directions along $(2\bar{2}1)_A$-$(\bar{2}21)_B$, $(1\bar{1}5)_A$-$(1\bar{1}1)_B$, and $(\bar{1}14)_A$-$(1\bar{1}4)_B$. Their relation to the second-order coincidence net is shown in Fig. 8. No other permissible boundaries, excepting combinations of these three, could be derived offering discontinuities susceptible to a con-

* A three-dimensional analysis would again include a permissible {110}-{110} boundary (in the plane of Fig. 8). Dunn, Daniels, and Bolton (18) mention such a boundary for Si-Fe.

siderable degree of trans-boundary restoration and having high coincidence site density.

The second-order twin join having a resultant direction along $(2\bar{2}1)$ of individual A and $(\bar{2}21)$ of individual B is shown in Fig. 9. The structure of A, above the discontinuity, is related to that of B, below the boundary, by a rotation of 38°57′ about a normal to the figure, [110]. The discon-

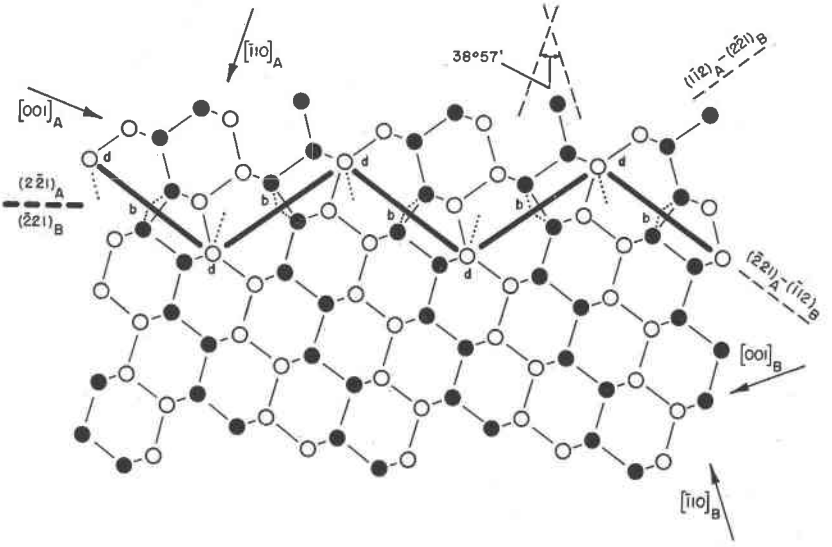

FIG. 9. {221}-{221} second-order twin join; see text for symbol explanation.

tinuity oscillates between segments having directions along $(1\bar{1}2)_A$-$(2\bar{2}1)_B$ and $(\bar{2}21)_A$-$(\bar{1}12)_B$. The projected atomic configurations along two adjacent segments of the proposed discontinuity show consecutive arrays having seven, five, seven, and five sides. At positions designated *b* in Fig. 9, two bonds have been rotated 19°28′ in the plane of the construction and combined to one; the resultant is 6% shorter than the normal bond. This particular deviation from undistorted bonding is present in all seven discontinuities referred to herein, i.e., in the four lateral twin boundaries discussed heretofore and in the three second-order twin joins presently being treated. At points *d*, the bond has been rotated alternately clockwise and counterclockwise by 31°35′ in the plane of the figure. Neglecting the shortened bond at *b*, atoms along the discontinuity maintain four nearest neighbors. This is in contrast with the four first-order boundaries, where atoms along the coincidence plane had alternately three and five nearest neighbors. See Table 1 and Fig. 1 for comparison with experimental results. The $\{221\}$-$\{221\}$ second-order twin

join has previously been encountered in silicon (cf. Fig. 4 of reference 4).

The second-order twin join shown in Fig. 10 has a resultant direction along $(1\bar{1}5)$ of individual A and $(1\bar{1}1)$ of individual B. The relation between A and B is the same as in the previous construction. The discontinuity oscillates between segments having directions along $(1\bar{1}2)_A$-$(2\bar{2}1)_B$ and $(\bar{1}14)_A$-$(1\bar{1}4)_B$. Adjacent segments show projected atomic configura-

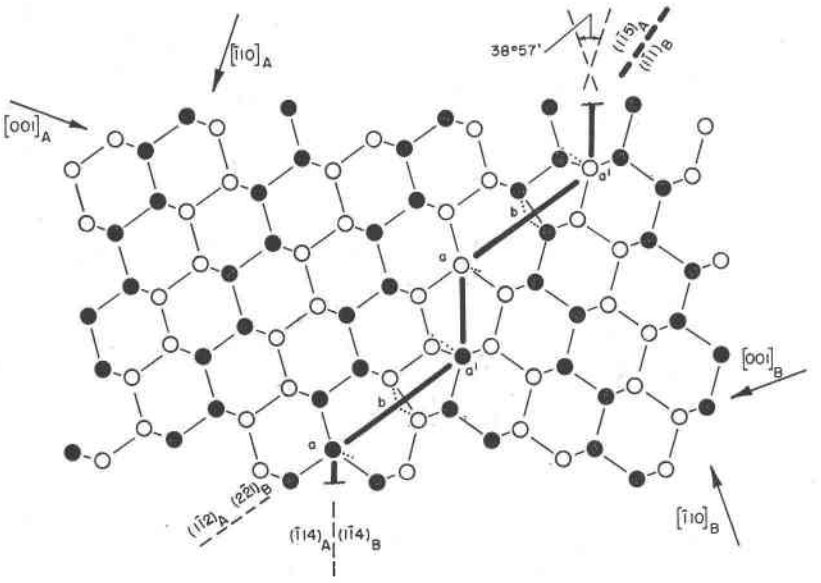

FIG. 10. {115}-{111} second-order twin join.

tions having seven, five, and six (altered) sides. The change in bonding at position *b* is the same as in the previous construction. The changes at *a* and *a'* are the same as at the similarly designated positions in the four first-order boundaries. The atoms at *a* require three nearest neighbors; those at *a'* require five. The two abnormally coordinated sites are separated by only 1.9 times the usual bond distance, permitting an adjustment of the structure to alleviate the condition. The deviations from undistorted bonding along the $\{115\}$-$\{111\}$ second-order twin join are the same, in both type and sequence, as those noted for the $\{115\}$-$\{111\}$ first-order boundary (Fig. 4). In fact, the only difference between these two discontinuities lies in the shapes of the arrays formed by projected trans-boundary atomic configuration. The $\{115\}$-$\{111\}$ second-order twin join is the only boundary discussed herein which was not observed in the silicon specimen studied.

The last zig-zag discontinuity for second-order twinning has a resultant

direction along $(\bar{1}14)$ of individual A and $(1\bar{1}4)$ of individual B; it is shown in Fig. 11. The boundary oscillates among segments having directions along $(1\bar{1}2)_A$-$(2\bar{2}1)_B$, $(\bar{1}14)_A$-$(1\bar{1}4)_B$, and $(\bar{2}21)_A$-$(\bar{1}12)_B$. The trans-boundary atomic configuration projected along two adjacent boundary segments shows arrays having seven, five, and six (altered) sides. The bonding changes at a, a', and b are the same as in the previous construc-

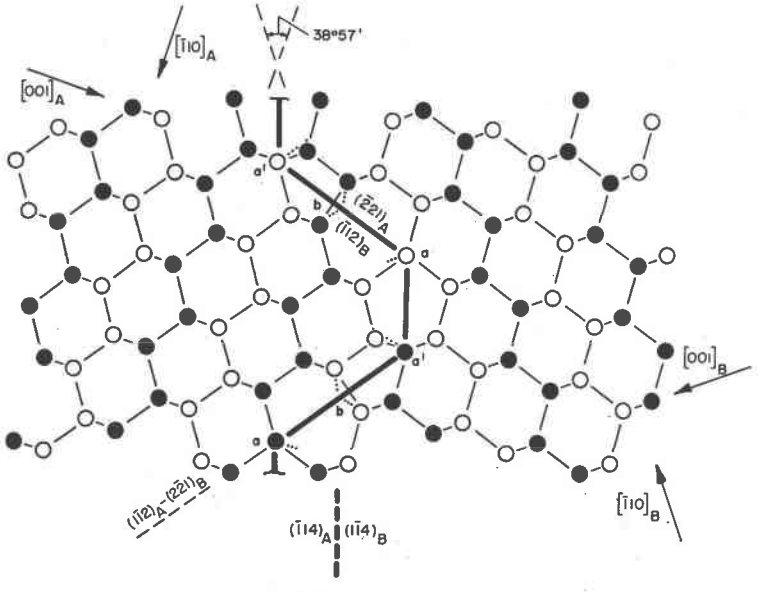

FIG. 11. {114}-{114} second-order twin join.

tion (Fig. 10); the boundary differs from that shown in Fig. 10 only in the direction reversals of the former. The trans-boundary structure of the $\{114\}$-$\{114\}$ second-order zig-zag discontinuity is also very similar to that of the $\{112\}$-$\{112\}$ first-order boundary (Fig. 5). See Table 1 and Fig. 1 for comparison with experimental results.

THIRD-ORDER TWINNING

The (110)-projected coincidence site superlattice for third-order twinning has approximately one-third the site density of the net derived by second-order twinning (Fig. 8). It consists of regions $1.3a_0$ wide, susceptible to structural restoration; these are separated by non-restorable areas $3.9a_0$ in width. No possibility exists for an $(h\bar{h}l)$ third-order twin join restorable along its entire length; partial restoration, however, is possible.

The boundaries designated III_1 in Fig. 1 and referred to in *Experimen-*

tal Results are apparently of the second-order type, i.e., they seemingly represent discontinuities between individual A (light gray) and B (black). When the observed boundary direction, however, was plotted on the coincidence site superlattice for second-order twinning, no restorable zigzag discontinuity could be constructed. Further examination of these areas was made in an attempt to account for the apparently anomalous behavior. High magnification revealed that an additional twinning was involved. Figure 12 is an enlargement of one of these areas (circled in Fig.

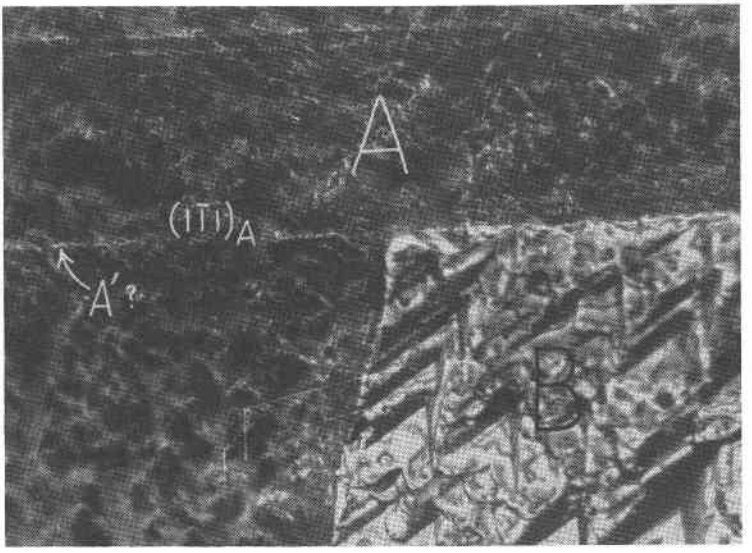

FIG. 12. Enlargement of circled area in Fig. 1, showing the additional twin lamella at the point of the "step." 470×.

1); the additional twin lamella can clearly be seen in individual A emanating from the point of the "step." Thus, the seemingly anomalous boundaries are not second-order twin joins. It was not clear, however, whether the thin lamella represented, on the part of individual A, a twinning back to the host orientation, or whether a new orientation, A′, had been generated. In the latter case, the boundary in question would be a third-order twin join, whereas if the former were true, it would be a first-order lateral twin boundary. *X*-ray diffraction was to no avail in deciding this point, since the lamella was too thin.

If individual A has twinned back to host orientation, it has done so by means of a $(1\bar{1}5)_H$-$(1\bar{1}1)_A$ lateral twin boundary. The resultant discontinuity between the host lamella and individual B is very close to a $(1\bar{1}4)_H$-$(1\bar{1}0)_B$ lateral twin boundary; the misfit is 3°41′. Examination of

the areas in question at magnifications up to 1000× failed to reveal any evidence for a boundary rotation of this amount. On the other hand, if the lamella represents a new orientation, A′, generated from A, the twin boundary (A:A′) involved is of the usual first-order type, i.e., $(1\bar{1}1)_A$-$(1\bar{1}1)_{A'}$ (Fig. 12). The resultant contact surface between individuals A′ and B, as stated above, is a third-order twin join, specifically $(1\bar{1}1)_{A'}$-$(\bar{1}\bar{1}\ 11\ 1)_B$. The latter discontinuity follows a row of sites in the third-order coincidence site superlattice. The boundary is restorable, in the sense used herein, along approximately 25% of its length. The latter explanation for these seemingly anomalous areas appears to be more plausible. From an animistic point of view, the silicon crystal, faced with the possibility of developing a non-restorable second-order twin join, twins again in order that the discontinuity (now third-order) achieve at least a certain degree of restoration; the lower energy state is selected. In this connection, Haasen (15) has noted in indium antimonide that twins of the same matrix sometimes twin again to "avoid direct contact with one another."

Fourth-order twinning in the diamond structure results in no lattice sites common to both individuals. Accordingly, trans-boundary restoration is lacking, and the discontinuity probably approaches that of a common (non-twin-related) grain boundary, i.e., a high-energy discontinuity.

Grain Boundary Energy

Read and Shockley (10), in their theoretical treatment of a boundary between two crystals which have a crystallographic direction in common and a small angular misfit, derived the relation

$$E = \frac{Ga(\cos\phi + \sin\phi)}{4\pi(1-\sigma)}\,\theta(A - \ln\theta)$$

for an isotropic cubic metal. E is the energy per unit area of the grain boundary, G represents the rigidity modulus, a is the lattice constant, ϕ is the inclination of the boundary from the symmetry position, σ is Poisson's ratio, θ represents the orientation difference between the lattices, and A is an arbitrary constant. In plotting E vs. θ, the theory calls for a rapid increase in energy with θ, followed by a less pronounced decrease. Excellent agreement is obtained with experimental determinations of relative grain boundary energy as a function of orientation, as carried out, for example, on silicon-iron (19), tin (20), lead (21), and silver (22). These data are summarized by Smith (23).

In the case of grain boundaries derived by twinning, the relative rotation angle, θ, is established, being 70°32′ for first-order twinning, 38°57′

for second-order, and 31°35′ for third-order. The various lateral twin boundaries and high-order twin joins offer different values of ϕ (grain boundary orientation) for constant values of θ. Read and Shockley (10) have shown that the E vs. θ curve contains low-energy cusps when the two crystals are in register on the same atom at regular intervals; the θ values corresponding to twinning orientations represent low-energy cusps. These authors have further reasoned that similar effects will be produced by varying ϕ, that is, large differences in energy are produced for a given θ by changes in orientation of the grain boundary. (They predicted energy cusps in first-order twin-related grains for $\{111\}$-$\{111\}$, $\{110\}$-$\{114\}$, and $\{112\}$-$\{112\}$; a cusp for the [second-order] twin join $\{221\}$-$\{221\}$ was also mentioned.) This conclusion has been borne out by experimentation. Lacombe (24), for example, noted that in aluminum the rate of boundary etching was strongly dependent upon the orientation of the boundary between twin grains, the attack on a $\{111\}$-$\{111\}$ twin boundary being relatively negligible; Shuttleworth, King, and Chalmers (25) had similar results with silver. Dunn, Daniels and Bolton (18) found an energy cusp for the $\{112\}$-$\{112\}$ twin boundary in silicon-iron and for a $\{110\}$-$\{110\}$ second-order twin join; they measured the energy of the $\{112\}$-$\{112\}$ boundary as 22 per cent of that of "ordinary boundaries." In copper, Fullman (26) measured the ratio of the interfacial free energy of coherent twin boundaries [$\{111\}$-$\{111\}$] to the "average grain boundary" free energy as 0.035. Fullman (27) also studied "noncoherent" twin boundaries in copper and found by measurement that a boundary "approximately parallel to a $\{113\}$ plane of one crystal and a $\{335\}$ plane of the other" had an interfacial free energy equal to 80 per cent of that of the "average grain boundary" free energy. In another paper, Fullman (28) measured the ratio of twin boundary energy [$\{111\}$-$\{111\}$] to "average grain boundary" energy in aluminum as 0.21.

The foregoing experimental data serve to establish that boundary orientation can have a decided effect on grain boundary energy. Further, higher energies are involved as one progresses through the boundary sequence wherein (*a*) twin plane and composition plane are coincident, (*b*) twin plane and composition plane are not coincident (lateral twin boundaries and high-order twin joins), and finally (*c*) the grains are unrelated by twinning. The boundaries proposed in the present study for diamond-type materials are of class (*b*). The four $(h\bar{h}l)$ lateral twin boundaries represent low energy cusps for $\theta = 70°32'$. Two are newly-proposed, $\{115\}$-$\{111\}$ and $\{001\}$-$\{221\}$; all have been experimentally observed (Fig. 1 and Table 1). The three $(h\bar{h}l)$ second-order twin joins correspond with low energy cusps for $\theta = 38°57'$. One is newly-proposed, $\{115\}$-

TABLE 2. DEVIATIONS FROM UNDISTORTED BONDING (ALONG BOUNDARY LENGTH OF 4.1 a_0)

	3‡ Nearest neighbors (symbol *a*)	5‡ Nearest neighbors (symbol *a'*)	*a*:*a'* Spacing	2 bonds to 1 at 19°28' 6% shortening (symbol *b*)	Undistorted 4 nearest neighbors (symbol *c*)	Distorted 4 nearest neighbors (symbol *d*)
{110}-{114}*	1	1	3.4§	1	3	0
{221}-{221}†	0	0	—	3	0	3.5
{115}-{111}*	2	2	1.9	2	0	0
{112}-{112}*	2	2	1.9	2	0	0
{115}-{111}†	2	2	1.9	2	0	0
{114}-{114}†	2	2	1.9	2	0	0
{001}-{221}*	1.75	1.75	3.4	1.5	1.5	0

* First-order.

† Second-order.

‡ The structure, of course, will adjust to alleviate these abnormal coordinations.

§ Times normal bond length.

Four of the listed boundaries show the same deviations from undistorted bonding and would accordingly have similar energies.

$\{111\}$; all but the latter have been experimentally observed (Fig. 1 and Table 1).

As stated previously herein, the energy of a particular grain boundary increases with the specific deviations from undistorted bonding. Such deviations are listed in Table 2 for the seven zig-zag discontinuities described in the present study.

SUMMARY

By an analysis of (110)-projected coincidence site superlattices in the diamond structure, seven permissible, "low-energy," $(h\bar{h}l)$ boundaries are derived and constructed; four refer to first-order twin-related grains and three to a second-order twin relationship. Two of the former and one of the latter are newly-proposed. The boundary directions follow rows of sites in the respective coincidence site superlattice. A considerable degree of trans-boundary structural restoration can be achieved if an oscillating, or *zig-zag* mechanism is used for the discontinuity surface. The seven $(h\bar{h}l)$ boundaries described for the diamond structure, and only these, are amenable to such restoration in addition to having high coincidence site density. Six of the discontinuities have been observed in the same silicon specimen, in addition to the normal $\{111\}$-$\{111\}$ boundary; *no others* were found for first- or second-order twinning.

Instances of probable third-order twinning have been noted in silicon.

The additional twin lamellae at these positions reflect the tendency of the crystal to avoid a non-restorable second-order twin join in favor of a partially-restorable third-order boundary.

Boundary orientation can have a pronounced effect on grain boundary energy. The seven structurally-restorable discontinuities described herein represent low-energy cusps in the curve relating energy and boundary direction, for constant misfit angles. Experimentation has previously shown that such boundaries are intermediate in energy between those in which twin plane and composition plane are coincident (usual case) and those involving a common, non-twin-related grain boundary.

Lateral twin boundaries and high-order twin joins in semiconductor materials are expected to affect structure-sensitive electrical properties, e.g., minority carrier lifetime and carrier mobility. Additionally, such boundaries, owing to their association with low-energy cusps, have a practical bearing upon semiconductor devices whose functioning depends upon high-energy grain boundaries.

Acknowledgments

The author is grateful to the following co-workers of these Laboratories: Mr. A. W. Petersen, Jr., for the preliminary Laue patterns; Mr. L. Toman, Jr., for preparing the silicon surface and for the two photomicrographs; Dr. W. Kaiser, for helpful discussions and for his critical review of the manuscript; and Drs. G. Wolff and H. Kedesdy, who also critically read the paper.

References

1. Mataré, H. F., and Reed, B., *Z. Naturforschg.* **11a,** 876–8 (1956).
2. Slawson, C. B. *Am. Mineral.* **35,** 193–206 (1950).
3. Kohn, J. A., *Ind. Diamond Rev.* **13,** 56–7 (1953).
4. Kohn, J. A., *Am. Mineral.* **41,** 778–84 (1956).
5. Mataré, H. F., Sylvania Electric Products, Inc., Bayside, L.I., N.Y., personal communication.
6. Kaiser, W., and Kohn, J. A., *Acta Met.* **4,** 220–1 (1956).
7. Ellis, W. C., and Treuting, R. G., *Jour. Metals* **3,** 53–5 (1951).
8. Mataré, H. F., *Z. Physik* **145,** 206–34 (1956).
9. Read, W. T., Jr., Dislocations in Crystals, McGraw-Hill, New York, 159 (1953).
10. Read, W. T., Jr. and Shockley, W., *Phys. Rev.* **78,** 275–89 (1950).
11. Teal, G. K., and Little, J. B., *Phys. Rev.* **78,** 647 (1950).
12. Keck, P. H., Van Horn, W., and MacDonald, A., *Rev. Sci. Instr.* **25,** 331–4 (1954).
13. Billig, E., *Jour. Inst. Metals* **83,** 53–6 (1954).
14. Greninger, A. B., *Trans. AIME* **122,** 74–120 (1936).
15. Haasen, P., *Jour. Metals* **9,** 30–2 (1957).
16. Churchman, A. T., Geach, G. A., and Winton, J., *Proc. Roy. Soc.* **238A,** 194–203 (1956).

17. SALKOVITZ, E. I., AND VON BATCHELDER, F. W., *Jour. Metals* **4,** 165 (1952).
18. DUNN, C. G., DANIELS, F. W., AND BOLTON, M. J., *Jour. Metals* **2,** 368–77 (1950).
19. DUNN, C. G., AND LIONETTI, F., *Jour. Metals* **1,** 125–32 (1949).
20. AUST, K. T., AND CHALMERS, B., *Proc. Roy. Soc.* **201A,** 210–15 (1950).
21. AUST, K. T., AND CHALMERS, B., *Proc. Roy. Soc.* **204A,** 359–66 (1950).
22. GREENOUGH, A. P., AND KING, R., *Jour. Inst. Metals* **79,** 415–27 (1951).
23. SMITH, C. S., *Inst. intern. phys. Solvay, 9th. Conseil, Brussels, État solide,* 11–53 (1951)
24. LACOMBE, P., Bristol Conf. on Strength of Solids (1947), published by Phys. Soc London (1948).
25. SHUTTLEWORTH, R., KING, R., AND CHALMERS, B., *Nature* **158,** 482–3 (1946).
26. FULLMAN, R. L., *Jour. Appl. Phys.* **22,** 448–55 (1951).
27. FULLMAN, R. L., *Jour. Appl. Phys.,* **22,** 456–60 (1951).
28. FULLMAN, R. L., *Gen. Elec. Co. Res. Rept.* No. **RL422,** Sept. 1950 (cf. p. 21 of reference 23).

Manuscript received July 29, 1957